

Numerical study of hydrodynamic and thermal behavior of Al_2O_3 / Water nanofluid and Al_2O_3 -Cu / Water hybrid nanofluid in a confined impinging slot jet using two-phase mixed model

M. Izadikia¹, M. Mahdi¹, K. Mobini¹

¹ Department of Thermal Sciences and Fluid Mechanics, Shahid Rajaee University of Tehran, Insert Postcode, Tehran, Iran.
 Phone: +982122970065 -; Fax: +982122970033

ABSTRACT – This study utilizes the two-phase mixture model to conduct a numeric study of Al_2O_3 /Water and Al_2O_3 -Cu/Water (hybrid) nanofluid's hydrodynamic and thermal behavior in a laminar confined impinging slot jet in $50 \leq \text{Re} \leq 300$ and nanoparticles volume fraction (NVF) ranging from 0-2% ($0 \leq \phi \leq 2\%$). This study considers various aspect ratios (H/W), including 2, 4, and 6, to investigate the confining effects. This paper gives a comparative analysis of nanofluids and hybrid nanofluids in terms of the parameters concerning the flow: Reynolds and local Nusselt number (Nux), average Nusselt number (Nuavg), flow lines' contour, and temperature distribution under similar geometric conditions and Reynolds number. In comparison with nanofluids, the hybrid nanofluids have higher local Nusselt number on the entire target surface, this advantage of hybrid nanofluid attribute to higher thermal conductivity. The average Nusselt numbers of nanofluids and hybrid nanofluids plotted at different Re for various aspect ratios (H/W=2,4), and the effect of aspect ratio and momentum are explained. Furthermore, pumping power of both fluid analysed for all nanoparticles volume fraction ($0 \leq \phi \leq 2\%$) at different Reynolds number. The result shows that pumping power of hybrid nanofluid is higher than base fluid and nanofluid, because the dynamic viscosity of hybrid nanofluid is higher than base fluid (water) and nanofluid. Besides, the study identified some correlations in the hybrid nanofluids regarding the stagnation point and the average Nusselt numbers. Presumably, these correlations are valid under certain conditions: $50 \leq \text{Re} \leq 300$, $2 \leq \text{H/W} \leq 6$, and $0\% \leq \phi \leq 2\%$.

ARTICLE HISTORY

Received: 13th Jan. 2021

Revised: 05th Apr. 2022

Accepted: 14th Apr. 2022

KEYWORDS

Impinging slot jet

Laminar flow

Two-phase mixed model

Hybrid nanofluid

Heat transfer coefficient

INTRODUCTION

Research studies in different fields have always focused on identifying new methods for improving heat transfer, applying two main approaches to this purpose: active and passive. Among; the active techniques, impinging jets have found wide applications since they offer high localized heat transfer coefficients (HTC); their applications include drying of textiles, film, and paper, temperature controlling of gas turbine components and combustors' outer wall, freezing of tissue in cryosurgery and manufacturing, material processing, and electronic cooling [1]. Many; recent research studies are interested in conducting numerical and experimental research on heat and mass transfer in impinging slot jets to investigate the various dimensions of this issue.

Although many researchers have conducted extensive research on impinging air jets, liquid jets have become the focus of more recent studies since they are useful in cooling heat engines, controlling the thermal condition of electronic devices, metals thermal treatment, and material processing.

Chiriac and Ortega [2] conducted a numerical study to investigate the unsteady fluid flow and heat transfer in a transitional, confined slot jet that impinged on an isothermal surface, and found that at steady flow, Re and Nu stagnation are correlated. Meaning that if Re value increases, the stagnation Nu increases in response Also; they found that the separation of flow resulting from the re-entrainment of the spent flow back into the jet can affect the transfer distribution in the wall jet region. Chiriac and Ortega also observed that the value of the heat transfer coefficient is associated with the steady/unsteady condition of the flow, since an extreme jump in the Re value to the supercritical limit results in an unsteady flow, leading to a higher HTC compared with under steady flow condition. Moreover; and slot jet does not represent any levels of unsteady effects. Li et al. [3] investigate a numerical study of a 2D laminar confined impinging slot jet about its flow field with two different outlet boundary conditions, in a specific range, the possibility of obtaining two different solutions for some geometric parameters and flow parameters. Observations; indicated the extreme impacts of different flow patterns on heat transfer. Similarly; in a numerical simulation, Sivasamy et al. [4] investigated the impingement flows of a 2-D laminar slot-jet, which was confined by a parallel wall, reporting its behavior based on the aspect ratio and Re. They said that, in the impingement and wall jet regions, Re and aspect ratio significantly impacted the bottom wall vorticity. Lee et al. [5] performed a numerical examination of a confined impinging slot jet concerning the fluid flow and heat transfer under different Re and heights ratios were, reporting the asymmetrical state and time-dependence of the flow and thermal fields in response to the Re surpassing a critical value. For the unsteady flow, by

increasing the Reynolds number, the flapping motion of the jet increases, and the flow fields become more complex with unsteady vertical movement caused by the augmentation of sinuous and varicose jet instability. In a relevant numerical investigation by Benmouhoub & Mataoui [6], the interactive connection between a moving horizontal isothermal hot wall with a turbulent plane jet, represented the considerably improving effect of the jet nozzle on the local heat transfer if the nozzle is inclined with an optimal angle in the opposite direction to the wall movement.

In a similar numerical study [7], concerning the thermal and fluid dynamic behavior of confined laminar impinging slot jets with nanofluids, the impacts of volume fractions of nanoparticles, various aspect ratios, and Re were examined in addition to the detection and presentation of specific correlations between the parameters of stagnation point and the average Nu. Furthermore; Lamraoui et al. [8] used a confined impinging slot jet to numerically examine a non-Newtonian Al₂O₃-water nanofluid flow's thermal behavior and fluid dynamic. That study set the following conditions for the Newtonian and non-Newtonian nanofluid flows $25 < Re < 300$ and $0 \leq \phi \leq 5\%$, revealing the positive relation between volume fraction of nanoparticles and Re and HTC as any increase in the former variables led to a similar effect in the latter. Moreover, the observations also indicated that, along the lower surface, the local Nu was higher in the non-Newtonian nanofluid compared to the Newtonian nanofluid. Analyzing; the steady-state, 2-D, Eulerian-Lagrangian model, Yousefi-Lafouraki et al. [9] studied the interactions between fluid-particle, and particle-wall (i.e., two-way coupling). The observations revealed the increasing effect of distance from the jet on the stability of the particle trajectory, which in turn improves Re. Furthermore; they detected a similar impact of the jet-impingement surface distance ratio on particle trajectory's stability when farther from the jet. Also; the results indicated that the mixture model had a higher HTC compared to the Eulerian-Lagrangian model. Abdelrehim et al. [10] conducted through numerical comparisons between single- and two-phase nanofluids models concerning the hydrodynamic and HT characteristics of a confined single impinging jet, based on whose results, it was revealed that the two-phase model had higher values for the local and average Nu with the maximum increase of 150% for $H/W = 4$ and $\phi = 4\%$. In another recent study, A numerical research [11] studied an incompressible confined slot jet impinging with nanofluid on an iso-thermal hot flat surface of a mini channel in a laminar fluid flow. That study also analyzed the water-based nanofluid with various nanoparticles in heat transfer performance: different particles included: Al₂O₃, SiO₂, Cu, Fe, diamond, and Ag. The results indicated the considerable effects of jet Re, the concentration of particles in the nanofluid, and the height to width ratio of the jet on fluid flow's heat transfer characteristics. Besides, the results also revealed that, in comparison with pure water, under $Re=300$ and particle concentration=5, HTP respectively represented 25% and 60% improvement in Al₂O₃-water and Cu-water nanofluids

In a curious experiment, Lee et al. [12] investigated the following: the characteristics of heat transfer and the general visualized the flow of confined, laminar milli-scale slot jets impinged on an isothermal flat target plate, with a fully-developed profile located at the nozzle exit. They studied the impacts of Re and the normalized nozzle-to-plate distance ratio (H/B); concluding that the local Nu decreases in response to an increase in the lateral distance from the stagnation point for all Re and H/B values. Hee Lee et al. [13] attempted to examine the impacts of Re, NDS (nozzle-to-surface distance), and the geometrical shape of target surface on local heat transfer in their experiment concerning the laminar heat transfer characteristics of a milli-scale confined slot jet impinging on concave and convex surfaces at a uniform heat flux. The results indicated that the local Nu for both surfaces increases in response to an increase in Re. While steadily decreasing in the wall jet region, the highest Nu for its axial distributions is located at the stagnation point. In a relevant experiment using Al₂O₃-water Jizu Lv et al. [14] researched a free single jet impingement to study the impacts of Re, nanoparticle volume fraction, NPD, and the impact angle on HTC. The observations indicated that the jet's heat transfer performance greatly improved when using Al₂O₃-water nanofluids, while HTC decreased along the radial direction, and when using different particle volume fractions. Barewar et al. [15] examined the heat transfer characteristics of an impinging free circular jet on the heated copper plate surface. They used two different coolants, including DI water and aqueous Zinc oxide nanofluids containing different nanoparticle concentrations. compared with water used as the coolant, HTC highly improved in Zinc oxide nanofluids coolant.

Approximately the entire papers published thus far concerning nanofluid-related topics, have defined it as a base fluid containing suspended nanoparticles made of only one material. Research; in this field often studies the impacts of various factors, including concentration, size, shape, and the material of the nanoparticles on nanofluids' thermo-physical characteristics, such as heat transfer, and pressure drop. Despite; the focus on using one type of material as a nanoparticle in many research studies, there has been a recent experimental attempt to investigate the employment of two types of dispersed nanoparticles called hybrid nanofluids.

The most critical positive characteristic of hybrid nanofluids, the possibility of merging two nanoparticle types dispersed in a base fluid, can improve HTR. Hence; a careful and intelligent selection of the material for these particles means they can complete each other's advantages and cover the setbacks. Alumina; which is a ceramic material, for example, is chemically immobile and substantially stable, which can be helpful to traits, whereas, in comparison with metal nanoparticles, Al₂O₃'s thermal conductivity is lower. Generally; metal nanoparticles, including copper, zinc, and aluminum, represent excellent thermal conductivity. Despite; the suitable thermal conductivity, the use of such materials is limited due to their stable and reactive properties. As a result, given the properties of metallic and non-metallic particles, it is possible to enhance this mixture's thermo-physical properties by using metal additives, like copper, to a nanofluid formed based on the Al₂O₃ nanoparticles [16].

Suresh et al. [17] designed an experiment to synthesize Al₂O₃-Cu/water as the hybrid nanofluid using a dual thermo-mechanical method to ensure the stability of this synthesized hybrid. That study used copper nanoparticles as additives

to the Al_2O_3 /water nanofluid, and the target product contained a range of different volume concentrations, such as 0.1%, 0.33%, 0.75%, 1%, and 2%.

W. Safiei et al. [18], discussed comprehensively about the flow of formulating nanofluid from preparation method, characterization, wettability analysis and stability techniques. Furthermore, the challenges for obtaining stable suspension and wettability behaviour of nanofluids are discussed as well. The main objective when preparing the nanofluids is to obtain a well-dispersed nanoparticle into the base fluid. Based on the literature review, the impact of surfactant on the stability and the correlation between nanofluids wettability and thermal-physical properties of nanofluids have great potential to discover. There are some aspects that can be considered to expand the knowledge of nanofluids such as the composition ratio of hybrid nanofluid with regards to achieving the best stability and wettability study of hybrid nanofluid with and without surfactant in the suspension.

W.H. Azmi et al. [19], review a comprehensive summary on thermo-physical properties and heat transfer application of oxide nanofluids. They evaluated that the oxide nanofluids were proven to perform better thermal properties and high enhancements in thermal conductivity with acceptable viscosity increments. Furthermore, the thermal conductivity of oxide nanofluids was enhanced up to 40% better than the base fluids and the forced convection studies using oxide nanoparticles for single and hybrid nanofluids showed significant improvements in heat transfer performance. It was reported in the literature with the heat transfer enhancement up to 60% with the use of oxide nanofluids in the heat transfer system.

Asif Khan et al. [20] investigated about the hydraulic and thermal performances of dissimilar particles of alumina silica/water hybrid nanofluid in a minichannel heat sink. Results indicate that the alumina/silica hybrid nanofluid can enhance heat transfer and pressure drop in a straight minichannel heat sink as compared with the base fluid (water).

Pascal Tiam Kapen et al. [21] investigated a stability analysis of $(\text{Cu}-\text{Al}_2\text{O}_3)$ /water hybrid nanofluid flow between two parallel and stationary plates filled with a porous medium. The effect of the density of particles, suction/injection Reynolds number, Hartmann number, Darcy number and volume fraction on the flow stability was examined. They found that the Darcy number affects the stability of the flow, the suction/injection reduces the drag and the transition is delayed/prevented, the magnetic field makes the dissipation very important because the kinetic energy of the electrically conductive fluid is absorbed by the Lorentz force, and the volume fraction and the density of nanoparticles increased the inertia of the fluid which decreased the speed gradient and damped the disturbances.

V. Murali Krishna et al. [22] study numerically fluid flow and heat transfer for flow of $\text{Cu}-\text{Al}_2\text{O}_3$ -water hybrid nanofluid in a microchannel heat sink (MCHS). The influence of Reynolds number and volume concentration of nanoparticles in $\text{Cu}-\text{Al}_2\text{O}_3$ /water hybrid nanofluid on MCHS performance is investigated. The results indicate an increase of 13.2% and 23.07% in Nusselt number for $\text{Cu}-\text{Al}_2\text{O}_3$ /water hybrid nanofluid compared with Cu /water and Al_2O_3 /water mono nanofluids respectively at 2.5% volume fraction. It is found from the numerical results that the pumping power requirement is less for hybrid $\text{Cu}-\text{Al}_2\text{O}_3$ /water nanofluid compared to Cu /water nanofluids and an increase of 430 Pa compared to pure water.

Given the mentioned benefits of using these hybrid nanofluids, they have the potential to become the next big player in nanofluid science, motivating more researchers to focus on and investigate hybrid nanofluids because of their impacts on heat transfer and the characteristics related to pressure drop.

Even though many research studies in the last couple of years have put their primary focus on the hydrodynamic and heat transfer behaviors of hybrid nanofluids inside horizontal ducts and sinusoidal corrugated enclosures and etc. [16, 22], using hybrid nanofluids to study confined slot jet impingement has caught almost no attention in the research field. Hence; this study attempts to fill this gap with the main aim of proposing a numerical solution for predicting Al_2O_3 /water nanofluid and Al_2O_3 - Cu /water hybrid nanofluid's hydrodynamic and thermal behavior for laminar confined slot jet impingement.

GOVERNING EQUATIONS

This research study has designed and conducted a 2-D CFD simulation of a confined slot-jet with an isothermal target surface the jet is vertically impinging using Al_2O_3 /water-based nanofluids and Al_2O_3 - Cu /water hybrid nanofluid. Figure (1) is a 2D representation of the simulated model in which W, H, and L respectively show jet width, the distance between the nozzle and the target surface, and the plate length. The study takes into account different geometric ratios (H/W) for defining the confining effects, considering the fluid flow as steady and laminar, and assuming different various jet velocities. The fluids used in the study include water- Al_2O_3 and water- Al_2O_3 - Cu with different nanoparticle volume fractions. Furthermore the diameter of a particle is 17nm. The used fluid is Newtonian and incompressible with assumed constant physical properties. Given; the mentioned assumptions, below you can find the conservation equations in two-dimensional coordinates:

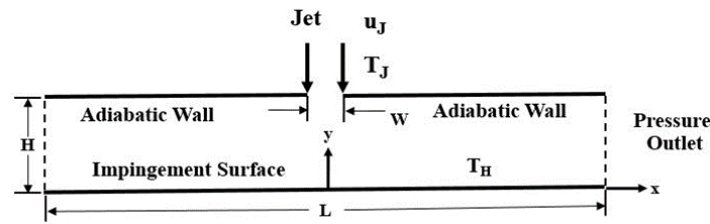


Figure 1. The geometric model with boundary conditions

Continuity equation:

$$\nabla \cdot (\rho_{eff} \vec{V}_m) = 0 \tag{1}$$

Momentum equation:

$$\nabla \cdot (\rho_{eff,o} \vec{V}_m \vec{V}_m) = -\nabla P + \nabla \cdot [\tau] + \nabla \cdot \left(\sum_{k=1}^n \phi_k \rho_k \vec{V}_{dr,k} \vec{V}_{dr,k} \right) \tag{2}$$

Energy equation:

$$\nabla \cdot \left(\sum_{k=1}^n \phi_k \vec{V}_k \rho_k E_k \right) = \nabla \cdot (K_{eff} \nabla T) \tag{3}$$

Volume fraction:

$$\nabla \cdot \left(\sum_{k=1}^n \phi_p \rho_p \vec{V}_m \right) = \nabla \cdot \left(\sum_{k=1}^n \phi_p \rho_p \vec{V}_{dr,p} \right) \tag{4}$$

Equation (5) and Eq. (6) allow for calculating shear stress and mean velocity:

$$[\tau] = \mu_{eff} \nabla \vec{V}_m \tag{5}$$

$$\vec{V}_m = \frac{(\sum_{k=1}^n \phi_k \rho_k \vec{V}_k)}{\rho_{eff}} \tag{6}$$

where ϕ_k is phase k's volume fraction. Moreover; the parameter $\vec{V}_{dr,k}$ in Eq. (2) is the drift velocity for the secondary phase k, (i.e., this study's nanoparticles), defined as below:

$$\vec{V}_{dr,k} = \vec{V}_k - \vec{V}_m \tag{7}$$

Besides, as shown in Eq.(8), the slip velocity, also known as the relative velocity, is described as the velocity of a secondary phase (p) relative to the primary phase (f):

$$\vec{V}_{pf} = \vec{V}_p - \vec{V}_f \tag{8}$$

Equation (9) expresses the relation of drift velocity ($\vec{V}_{dr,k}$) to relative velocity:

$$\vec{V}_{dr,k} = \vec{V}_k - \frac{(\sum_{k=1}^n \phi_k \rho_k \vec{V}_{fk})}{\rho_{eff}} \tag{9}$$

The correlation introduced in this study [23] is useful for calculating relative velocity:

$$\vec{V}_{pf} = \frac{\rho_p d_p^2}{18 \mu_f f_{drag}} \frac{\rho_p - \rho_{eff}}{\rho_p} \vec{a} \tag{10}$$

where f_{drag} represents the drag function. correlation proposed by Schiller and Naumann [24] determines drag function; this correlation is depicted in Eq.(11):

$$f_{drag} = \begin{cases} 1 + 0.15 Re_p^{0.687} & Re_p \leq 1000 \\ 0.0183 Re_p & Re_p > 1000 \end{cases} \tag{11}$$

In the above equation, the parameter Rep is equal to $\frac{\bar{v}_m d_p}{\nu_{eff}}$.

Besides, in Eq. (10), the acceleration vector (\vec{a}) is defined as:

$$\vec{a} = \vec{g} - (\vec{V}_m \cdot \nabla) \vec{V}_m \tag{12}$$

(HYBRID) NANOFLUIDS' THERMAL AND PHYSICAL PROPERTIES

By the equations mentioned thus far, Eqs. (13-24), it is possible to determine nanofluids and hybrid nanofluids' thermophysical properties, including Al_2O_3 /water nanofluid's viscosity, density, specific heat, and thermal conductivity. The experiment by Suresh et al. [17], which used a two-phase mixed model, provided sufficient data concerning the thermo-physical properties of Al_2O_3 -Cu/water hybrid, which are valid for nanoparticles with an average diameter of 17 nm. Table 1 presents the relevant data regarding these physical properties in that experiment. The effective density is calculated as follows:

$$\rho_{eff} = \phi \rho_p + (1 - \phi) \rho_f \tag{13}$$

As seen in Eq. (14), this study's [25] proposed expression can be useful for determining TEC (Thermal expansion coefficient):

$$\beta_{eff} = \left[\frac{1}{1 + \frac{(1 - \phi) \rho_f \beta_f}{\phi \rho_p}} + \frac{1}{1 + \frac{\phi \rho_p}{(1 - \phi) \rho_f}} \right] \times \beta_f \tag{14}$$

The expression proposed by Chon et al. [26] is useful for calculating the effective thermal conductivity, as in the form of Eq. 15, which considers the mean diameter of nanoparticles and the Brownian motion:

$$\frac{K_{eff}}{K_f} = 1 + 64.7 \phi^{0.746} \left(\frac{d_f}{d_p} \right)^{0.369} \left(\frac{K_p}{K_f} \right)^{0.7476} Pr^{0.9955} Re^{1.2321} \tag{15}$$

The following equations describe Pr and Re in Eq. (15):

$$Pr = \frac{\mu}{\rho_{BF} \alpha} \tag{16}$$

$$Re = \frac{\rho_{BF} K_b T}{3\pi \mu^2 L_{BF}} \tag{17}$$

In these equations, LBF is the mean free path of water. At laboratory temperature, the value of the water mean free path is 0.17 nm. Also; the Boltzmann constant (1.3807×10^{-23} J/K) is represented by K_b while Eq. (18) determines μ :

$$\mu = A \times 10^{\frac{B}{T-C}} \quad C = 140 \quad B = 247 \quad A = 2.414e - 5 \tag{18}$$

Masoumi et al. [27] recently introduced a new expression through Eq.(19) to predict nanofluids' effective viscosity. Viscosity is dependent on the following parameters, including nanoparticles volume fraction, mean nanoparticle diameter, temperature, nanoparticles density, and the based fluid physical properties:

$$\mu_{eff} = \mu_f + \frac{\rho_p V_B d_p^2}{72C\delta} \tag{19}$$

where the parameters of V_B and δ respectively, indicate the nanoparticle's Brownian velocity and the distance between the particles. These two parameters are determinable using the following equations:

$$V_B = \frac{1}{d_p} \sqrt{\frac{18K_b T}{\pi \rho_p d_p}} \tag{20}$$

$$\delta = \sqrt[3]{\frac{\pi}{6\phi}} d_p \tag{21}$$

Besides, in Eq.(19), the parameter of C is defined as below:

$$C = \mu_f^{-1}[(c_1 d_p + c_2) \phi + (c_3 d_p + c_4)] \quad (22)$$

Where the constants c_1 - c_4 are equal to:

$$\begin{aligned} c_1 &= -0.000001133. c_2 = -0.000002771 \\ c_3 &= 0.00000009. c_4 = -0.000000393 \end{aligned} \quad (23)$$

Table 1. Thermal and physical properties of nanofluid and hybrid nanofluid at inlet temperature [17]

$\phi(\%)$	$K_{nf}(W/m-K)$	$\mu_{nf}(kg/m-s)$	$K_{hnf}(W/m-K)$	$\mu_{hnf}(kg/m-s)$
0.1	0.614055	0.0009041	0.6199817	0.000972
0.33	0.6190041	0.0009049	0.6309797	0.001098
0.75	0.6309797	0.0009098	0.6490042	0.001386
1	0.6437496	0.00095184	0.6570083	0.001602
2	0.6571916	0.000972	0.6849921	0.001935

Table 2. Thermal and physical properties of water and Al_2O_3 at inlet temperature [7]

Material	$\rho(kg/m^3)$	$C_p(J/kg.K)$	$K(W/m-K)$	$\mu(kg/m-s)$
water	997.7	4180	0.613	0.000885
Al_2O_3	3880	880	36	-

GEOMETRIC MODEL AND DATA SIMPLIFICATION

Figure 1 is a 2D representation of the simulated model of the confined impinging slot jet. The target surface and the upper adiabatic wall are 620 mm long, while for the aspect ratios (H/W) of 2, 4, and 6, the values of distance between the surfaces (H) are respectively 12.4, 24.8, and 37.2 mm. While the nozzle width (W) is 6.2 mm, the study considered the temperature at the stationary target surface to be constant (313 K) and used the pure water, Al_2O_3 /water nanofluid, and Al_2O_3 -Cu/water hybrid nanofluid as fluids for the simulation. The study used Re, Nu, and dimensionless temperature to simplify data. Eqs. (24-26) determine these parameters:

$$Re = \frac{\rho u_j W}{\mu} \quad (24)$$

$$Nu = \frac{\dot{q}W}{(T_H - T_j)K_f} \quad (25)$$

$$\theta = \frac{T - T_j}{(T_H - T_j)} \quad (26)$$

In the above equations, the parameters u_j , W and \dot{q} are respectively the jet mean velocity, jet width, and heat flux measured on the target surface. In addition, the temperatures, T_H and T_j , are the target surface and inlet jet temperatures, respectively.

The boundary conditions used in the simulation are described as follows:

- Jet input section: $T = T_j$, $u = u_j$
- target surface ($y=0$): $T = T_H$
- The upper adiabatic wall: $\frac{\partial T}{\partial y} = 0$
- Output sections $P = P_{atm}$

NUMERICAL PROCEDURE

The study used Ansys FLUENT to solve the fluid flow's discretized governing equations numerically and implicitly linearized the governing equations following equations' dependent variables and solved them under steady conditions. Then, the study utilized the second-order upwind scheme and the SIMPLE algorithm for equations concerning the energy and momentum for handling the pressure-velocity coupling. For velocity and energy equations, the study respectively considered the convergence criteria of 10^{-5} and 10^{-8} , considering the ambient temperature (293K) as an assumption for the inlet fluid flow. For various inlet uniform velocities, the fluid flow is laminar as $100 < Re < 300$, u_j is considered in the simulation. The study did not consider any slip condition for the wall boundaries while considering the velocity inlet

and pressure outlet conditions for inlet and outlet boundaries. Although; setting the upper wall to be adiabatic, the study fixed a uniform constant temperature for the target surface.

The grid independence study was carried out by considering four different grid distributions on the model with a dimensional ratio (H/W) of 4 and Re of 100 and pure water as the working fluid. The study created the experiment models with the following nodes in this order: 5472 (95x55), 19729 (180x110), 73944 (710x100), and 284200 (1420x200) nodes, and structured the grid mesh. Nu variations at the bottom wall using a fine mesh grid are illustrated in Figure 2. The grid tends toward independence for a mesh grid with 710x100 nodes. Hence; the study selected the third mesh grid for simulation. This selection has the advantage of reducing the required time for calculation time, thus, functioning to the benefit of results' accuracy.

Sadly, this study could not detect existing substantial and authentic data regarding experiments or numerical investigation of fluid flow parameters in the confined impinging slot jet in the context of hybrid nanofluid for numerical authentication of its results; thereby, it had to use the results of the following studies, conducted for air or nanofluid, as the criteria against which to validate its results: Li et al. [3] , Lee et al. [12], and Manca et al. [7].

In the first validation, the study compared the variation of $Nu/Re^{0.5}$ along the target surface, with air as the working fluid, with the results provided by Li et al. [3] to ensure the accuracy of this numerical method, as depicted in Figure 3a. Based; on the results of this comparison, with a maximum error of about 5.78%, the study detected a significant agreement between the results of the two studies.

The study compared the range of differences of Nu with air as the working fluid along the target surface with the results of a relevant experiment [12]in the second validation. Figure 3(b) presents a comparison of this study's results and the consequences of that experiment, which represent a significant closeness.

The study compared the results obtained by Manca et al. [7] with the results for the two solid volume fractions ϕ (0 and 5%) at $Re = 100$ in the third validation. Figure 3(c) and Figure 3(d) depicts the simulation results of this study concerning the local Nu along the target surface with the relevant study mentioned, indicating subtle differences. The maximum errors for $\phi = 0\%$ and $\phi = 5\%$ are respectively about 7.15% and 5.56% in this comparison.

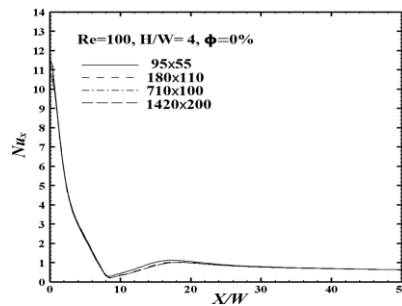


Figure 2. The grid independence results: local Nu along the target surface

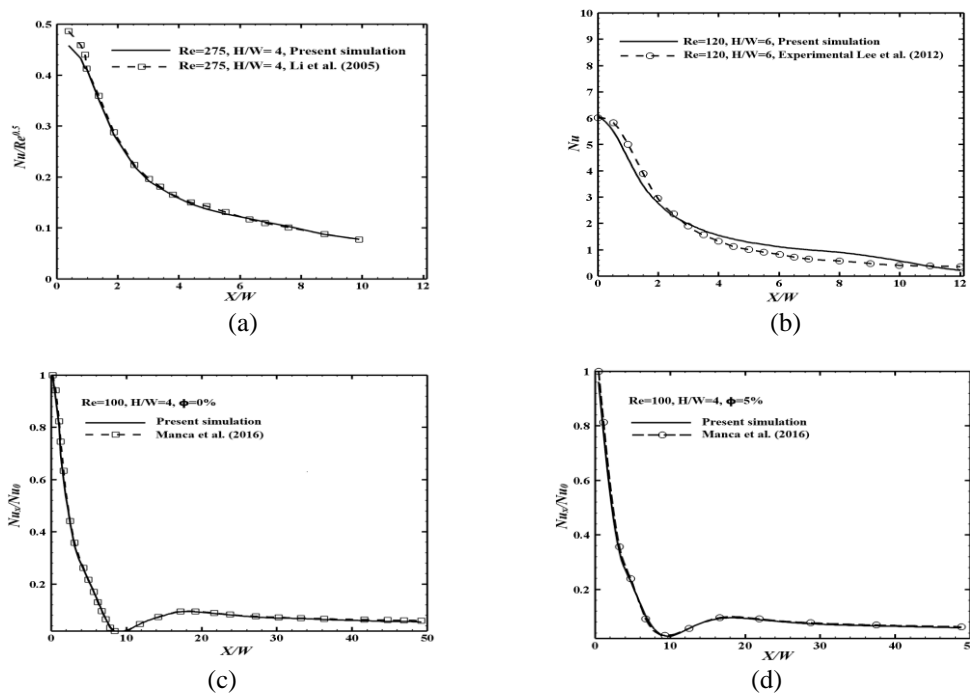


Figure 3. Authentication of this study's results via a comparison of the Nu values along the impingement surface in related research

RESULTS AND DISCUSSION

Figure 4 to Figure 7 represent the local Nu along the target surface for water, nanofluid, and hybrid nanofluid under the following conditions: Re of 100 and 200, volume fractions of 1% and 2%, and aspect ratios of 4 and 6. Regarding; the symmetry condition at $x = 0$ around the jet axis, on the right side of the target wall, the local Nu distribution diagram is plotted. Based on the data presented by Figure 4 and Figure 5, the local Nu on the lower surface is 30% higher for hybrid nanofluid than the base fluid (water), under ($\phi=1\%$ and $Re = 100$ and 200), while this value is 6% for nanofluid. Hybrid nanofluids are more effectively conductive, thus, having a higher local Nu . The obtained Nu values in this study ranged from the highest to lowest, as depicted by Figure 4 and Figure 7. The following lines discuss this in more detail. Based on observations, a report of which is presented in Figure 6 and Figure 7, hybrid nanofluid' local Nu along the target surface under ($\phi = 2\%$ and $Re = 100$ and 200) is 40% higher in comparison with pure water, which is the base fluid. The same value for the nanofluid, though, is 7% higher. These observations suggest that in the hybrid nanofluid's volume fraction of nanoparticles is more influential than in nanofluid.

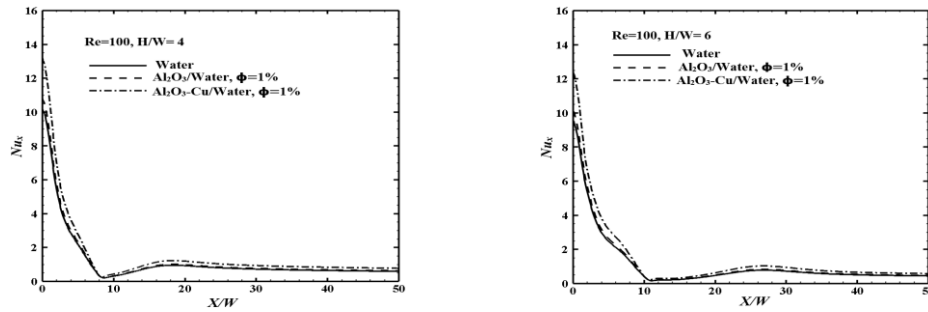


Figure 4. A comparison of the local Nu on the lower surface between water, nanofluid and hybrid nanofluid for H/W (4 and 6), $Re = 100$ and $\phi = 1\%$

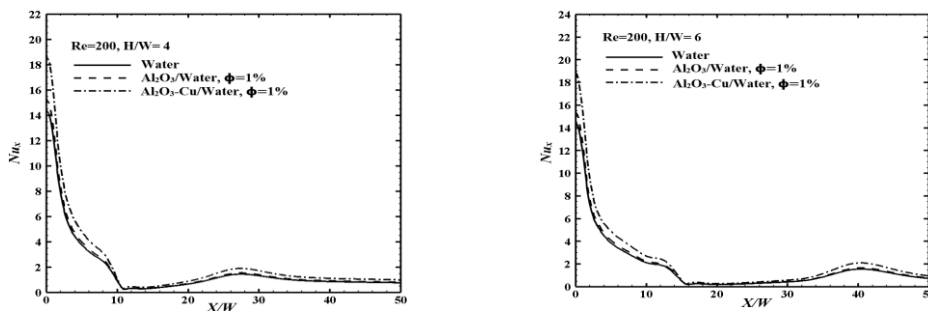


Figure 5. A comparison of the local Nu on the lower surface between water, nanofluid and hybrid nanofluid for H/W (4 and 6), $Re = 200$ and $\phi = 1\%$

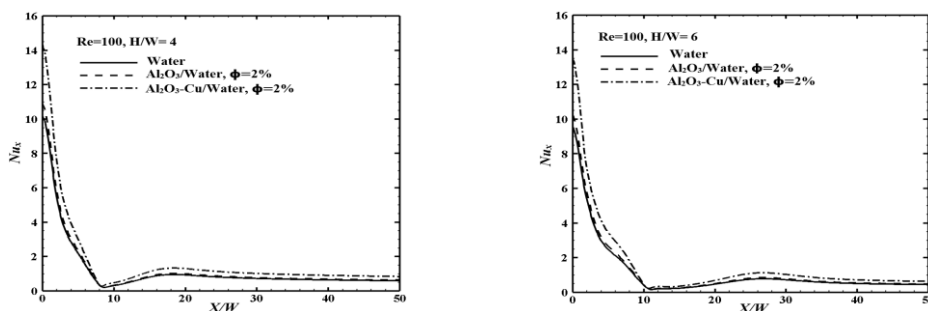


Figure 6. A comparison of the local Nu on the lower surface between water, nanofluid and hybrid nanofluid for H/W (4 and 6), $Re = 100$ and $\phi = 2\%$

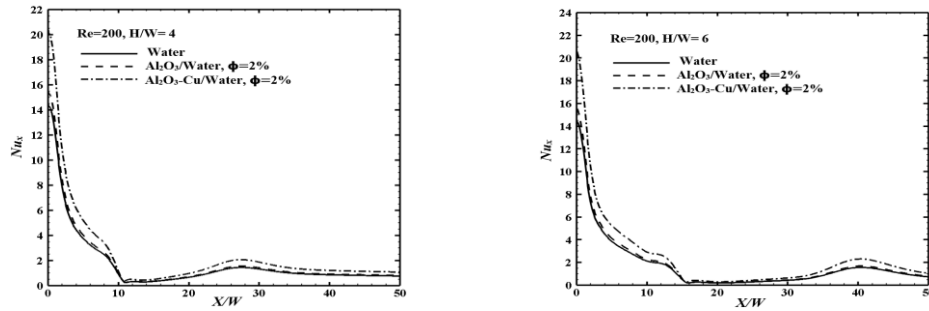


Figure 7. A comparison of the local Nu on the lower surface between water, nanofluid and hybrid nanofluid for H/W (4 and 6), $Re = 200$ and $\phi = 2\%$

Regarding the considerable effect of laminar and turbulent flows and fluid properties on heat transfer, this study investigated the distribution of streamlines, and thermal boundary layer contours for hybrid nanofluids. Figure 8 illustrates the hybrid nanofluid's streamlines under Re values of 100 and 200, aspect ratios of 2, 4, and 6, and $\phi = 2\%$. Observations; reported two small vortices with opposite rotation near the jet axis and the upper wall. Since the vortices for $Re = 200$ are stretched to the downstream exit of the jet, compared with those under $Re = 100$, they are larger, thus raising the convective force. As depicted in the figure, the rising in the values of Nu leads to the early occurrence of flow separation and the emergence of secondary vortices near the bottom wall. Under $Re = 100$ and $H/W = 4$, for example, the occurrence of the inner vortex is observed between $x/W = 8$ and $x/W = 16$, which leads to the separation and re-attachment of the flow, thereby resulting in the minimum and maximum heat transfer coefficient values in the related profiles.

Figure 9 represents hybrid nanofluids' temperature distribution ($\phi = 2\%$) at different H/W and Re values. As presented in the diagrams, the stagnation zone represents the highest temperature gradients. At the separation zone, the lowest temperature gradients are observable, hence; the highest and the lowest heat transfer rate (HTR) values in the two zones. We expect, for example, to observe the maximum thermal boundary layer thickness at $x/W \approx 11$ for $Re = 100$ and $H/W = 4$, leading to the lowest heat transfer coefficient and Nu . The decreasing trend of the thermal boundary layer begins after re-attachment of the flow, at about $x/W \approx 16$, in response to which the heat transfer coefficient and Nu increase.

The application of nanofluid or hybrid nanofluid raises the fluid bulk temperature through an enhanced thermal conductivity and a more effective heat transfer capability. The comparison between the behavior of nanofluid and hybrid nanofluid suggests that hybrid nanofluids have a thinner thermal boundary layer, leading, in turn, to a greater heat transfer coefficient in a hybrid nanofluid.

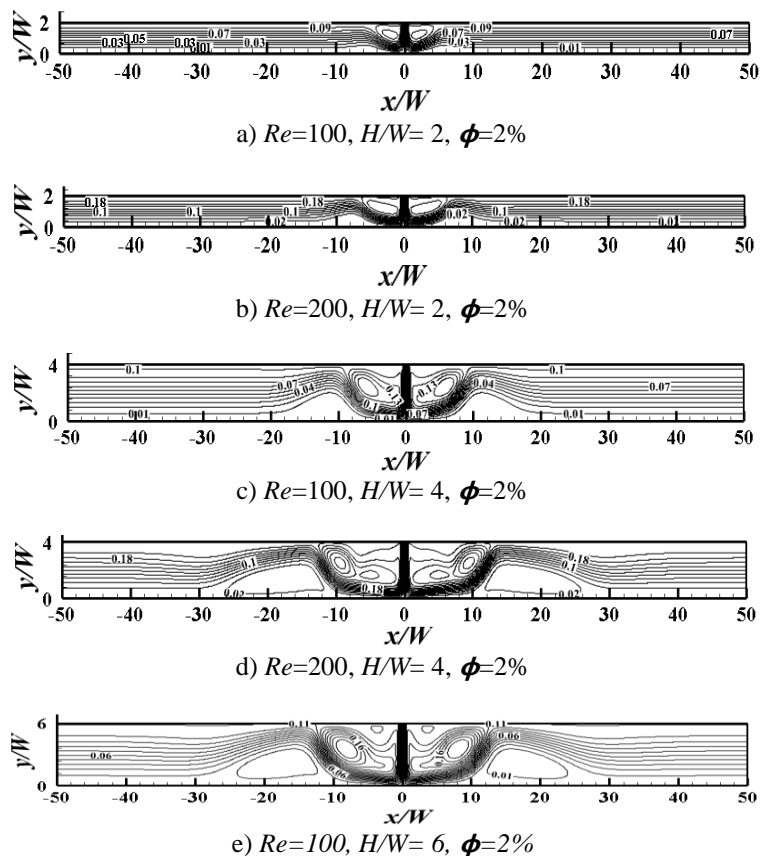
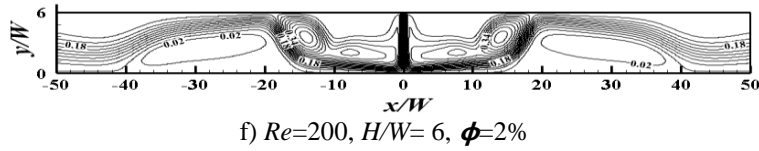
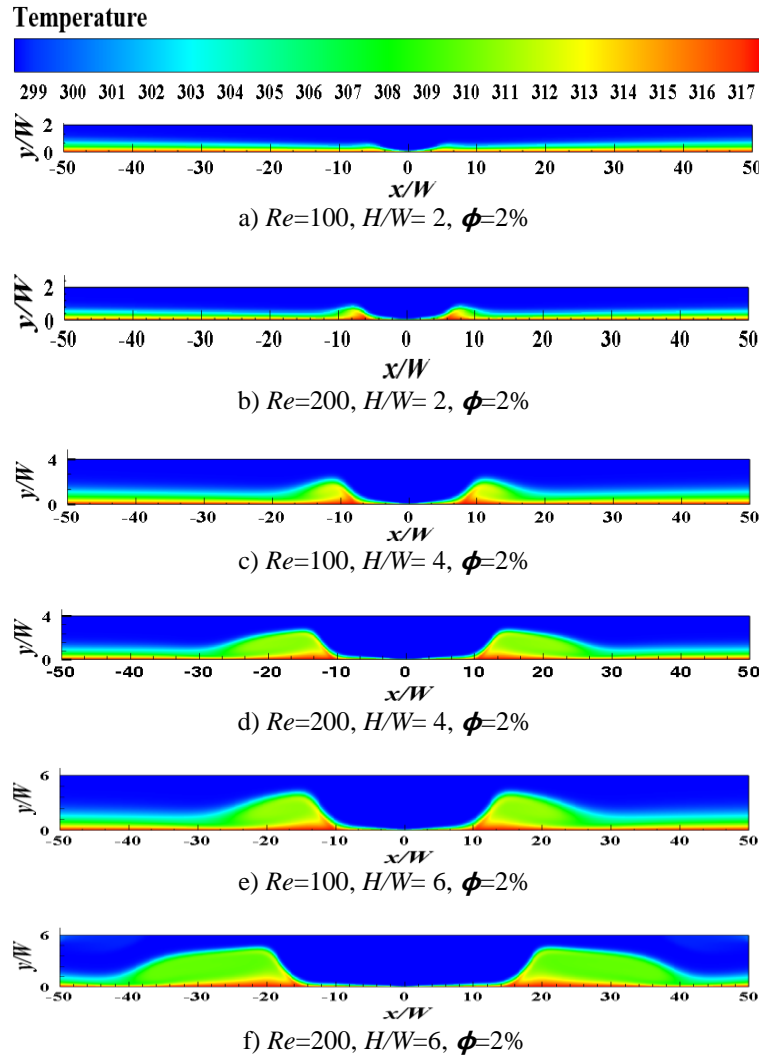


Figure 8. The hybrid nanofluids' stream function contours for $\phi = 2\%$, $Re = 100$ and 200 and $H/W = 2, 4$ and 6



f) $Re=200, H/W= 6, \phi=2\%$

Figure 8. The hybrid nanofluids' stream function contours for $\phi = 2\%$, $Re= 100$ and 200 and $H/W = 2, 4$ and 6 (cont.)



a) $Re=100, H/W= 2, \phi=2\%$

b) $Re=200, H/W= 2, \phi=2\%$

c) $Re=100, H/W= 4, \phi=2\%$

d) $Re=200, H/W= 4, \phi=2\%$

e) $Re=100, H/W= 6, \phi=2\%$

f) $Re=200, H/W=6, \phi=2\%$

Figure 9. Hybrid nanofluids' temperature distribution at $\phi = 2\%$, $Re=100$ and 200 and $H/W = 2, 4$ and 6

The values of Nu_{avg} as a function of ϕ , in $Re = 50, 100, 200$ for the dimensional ratio ($H/W = 4,6$) are shown in Figures (10) and (11), respectively. The results show that Nu_{avg} for nanofluid and hybrid nanofluid increases with increasing Re and ϕ . This is due to the increase in displacement by increasing the Re number and the increase in the effective thermal conductivity of the nanofluid and the hybrid nanofluid with ϕ , respectively. The average Nusselt number for hybrid nanofluid is higher than nanofluid and the difference in Nu_{avg} of these two different fluids is due to the higher thermal conductivity of nanofluid hybrids than nanofluids. For example, for $Re = 100$ and $H/W = 4$, Figure (11) shows that for a hybrid nanofluid, Nu_{avg} is 1.51 and 1.65 at $\phi = 1\%, 2\%$, respectively. Under the same conditions, for nanofluids, Nu_{avg} is 1.25 and 1.26, respectively. Table (2) shows the values of Nu_{avg} for all conditions. For a fixed Reynolds, when the H/W increases from 4 to 6 jets of fluid to travel more to hit the bottom plate, so the fluid temperature decreases when it hits a hot plate along the way, so Nu_{avg} at $H/W = 4$ is greater than the $H/W = 6$ values at $Re = 50, 100$, which is quite evident in the table for nanofluids and nanofluid hybrids. if $Re = 200$, the fluid momentum is increased, and when the H/W changes from 4 to 6, the average Nusselt number changes are very small and close to each other, this physical change is due to the increase in fluid momentum which increases H/W makes almost ineffective.

Illustrated in Figure 10 and Figure 11 are the variations of Nu_{avg} as a function of ϕ under (Re of 50, 100 and 200) and aspect ratios of 4 and 6. Based on the results, in nanofluid and hybrid nanofluid, Nu_{avg} increases in response to increasing Re and ϕ values due to nanofluids and hybrid nanofluids' increased Re and thermal conductivity following an increase in the concentration of nanoparticles. The comparison between the results represented that nanofluids have a lower Nu_{avg} than hybrid nanofluids. Basic on of the data in Figure 11, it is observed that under ($Re = 100, H/W = 4$), Nu_{avg} is 1.51 at

$\phi=1\%$ and 1.64 at $\phi=2\%$ for hybrid nanofluid. Besides, at ($Re = 100$), and ($\phi=1$ and 2%), Nu_{avg} is respectively 1.25 and 1.26 .

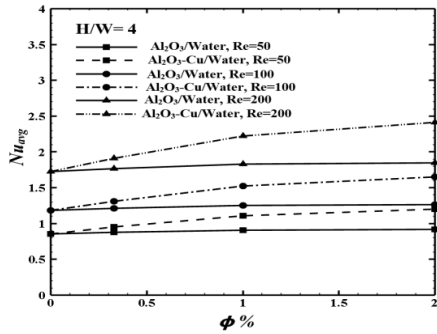


Figure 10. Variation of the average Nusselt number as a function of ϕ for nanofluid and hybrid nanofluid at $Re=50, 100, 200$ and $H/W = 4$

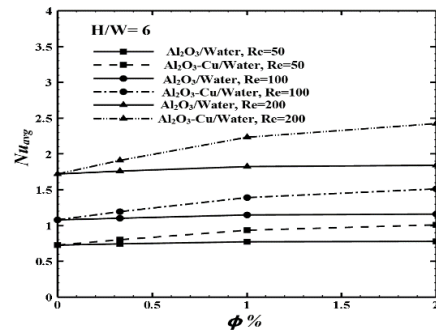


Figure 11. Variation of the average Nusselt number as a function of ϕ for nanofluid and hybrid nanofluid at $Re=50, 100, 200$ and $H/W = 6$

Table 3. The average Nusselt number of nanofluids and hybrid nanofluid

H/W=6			H/W=4				Re	ϕ (%)
Nanofluid Nu_{avg}			Nanofluid Nu_{avg}					
200	100	50	200	100	50	0		
1.719187	1.079233	0.727	1.724665	1.181662	0.85621	0.33		
1.761587	1.105314	0.744	1.765615	1.209494	0.87598	1		
1.825801	1.146077	0.771	1.829834	1.253527	0.907781	2		
1.844011	1.158424	0.78	1.847975	1.266021	0.916553			
Hybrid Nanofluid Nu_{avg}			Hybrid Nanofluid Nu_{avg}				Re	ϕ (%)
200	100	50	200	100	50	0.33		
1.911347	1.196998	0.805	1.912854	1.310292	0.95	1		
2.231676	1.391325	0.935	2.224171	1.522437	1.106289	2		
2.42679	1.510051	1.01	2.413686	1.651407	1.20065			

Taking into account the system pumping power and pressure drop is a vital step for ensuring a more efficient investigation. The necessary pumping power is calculated from $Q \times \Delta p$. This section discusses the pumping power needed for various Re values and different concentrations of nanoparticles in both nanofluid and hybrid nanofluid. Figure (12) shows the nanofluid pumping power (PP_{nf}) in terms of Reynolds number for the volume fraction of nanoparticles at ($H/W = 2$). According to the diagram, it can be seen that with increasing concentration from $\phi = 0\%$ to $\phi = 2\%$, the pumping power increases. Physically, as the concentration of nanoparticles increases, the dynamic viscosity of the nanofluid increases [7,8] and as a result more pumping power is required. For example, by increasing the concentration of nanoparticles from $\phi = 0\%$ to $\phi = 2\%$ in Reynolds ($Re = 100$), the pumping power changes from 1.7×10^{-3} W to 2.23×10^{-3} W. Similarly, for hybrids nanofluid, the same analysis can be applied, with the difference that the changes in dynamic viscosity and pumping power for hybrids nanofluid are greater than nanofluids due to the experimental work done [17]. Figure (13) shows the pumping power of the hybrid nanofluid in terms of Reynolds number and the pumping variations are greater than the nanofluid.

Figure 14 depicts the pumping power ratio variation for nanofluid (PP_{nf}) to pumping power for the base fluid (PP_{bf}) as a function of Re for various nanoparticle concentrations at $H/W = 2$. The dynamic viscosity increases in the base fluid with the addition of nanoparticles, resulting in a higher pumping power ratio for both nanofluids and nanofluid hybrid compared with the base fluid. At $\phi = 2$, for example, the nanofluid and hybrid nanofluid's dynamic viscosity are calculated 1.14 and 2.26 times the base fluid's viscosity, proposing the Re -independent characteristic of this ratio. A comparison of the results depicted in Figure 14 and Figure 15 shows the hybrid nanofluid's considerably higher pumping power ratio than the nanofluid due to the higher dynamic viscosity of the former than the latter. For instance, the dynamic viscosity in hybrid nanofluid is two times higher than nanofluid at $\phi = 2\%$.

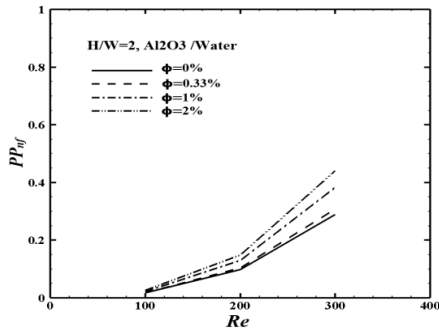


Figure 12. Pumping power for nanofluid versus Re at $\phi = 0, 0.33, 1, 2\%$ and $H/W = 2$

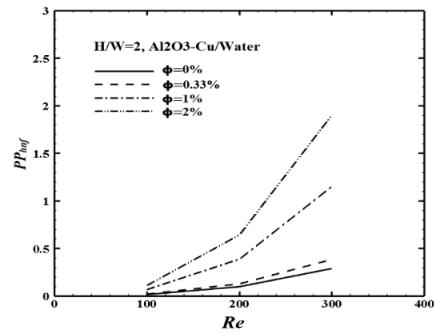


Figure 13. Pumping power for hybrid nanofluid versus Re at $\phi = 0, 0.33, 1, 2\%$ for $H/W = 2$

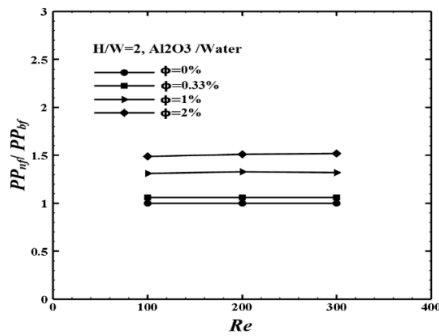


Figure 14. Pumping power ratio for nanofluid versus Re at $\phi = 0, 0.33, 1, 2\%$ and $H/W = 2$

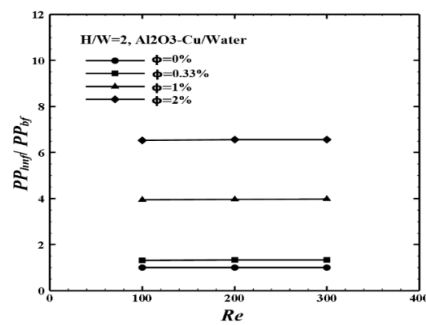


Figure 15. Pumping power ratio for hybrid nanofluid versus Re at $\phi = 0, 0.33, 1, 2\%$ for $H/W = 2$

The Nu at stagnation point and the average Nusselt number are related to the jet Re and the H/W ratio for (water) the base fluid. In Eq. (27), the correlation obtained from the least squared curve fittings of the obtained numerical data is represented as below:

$$Nu = aRe^b(H/W)^c \tag{27}$$

Besides, these correlations are obtained and drawn in Figure 14(a), which are valid when $100 \leq Re \leq 300$ and $2 \leq H/W \leq 6$:

$$Nu_0 = 1.122 Re^{0.4926} (H/W)^{-0.0414} \tag{28}$$

$$Nu_{avg} = 0.3418 Re^{0.4019} (H/W)^{-0.4436} \tag{29}$$

The SD values of the stagnation point and the average Nu correlations are respectively 1% and 5%. Besides, the regression coefficient (R^2) in Eq. (28) and Eq. (29) are respectively 0.999 and 0.992. When employing the hybrid nanofluid, a correlation for the ratio of stagnation point and the average Nusselt numbers for the base fluid can be expressed as Eq. (30), which is a function of the concentration of nanoparticles.

$$Nu_{hnf}/Nu_{bf} = a + \phi(b + c\phi + d\phi^2) \tag{30}$$

Moreover, under $100 \leq Re \leq 300$ and $2 \leq H/W \leq 6$, the obtained equations depicted below in Figure 16(b) are valid.

$$Nu_{0,hnf}/Nu_{0,bf} = 1 + \phi(37.17 - 772.8\phi - 2969\phi^2) \tag{31}$$

$$Nu_{avg,hnf}/Nu_{avg,bf} = 1 + \phi(36.59 - 836.9\phi + 106.1\phi^2) \tag{32}$$

The standard deviations of the stagnation point and the average Nu correlations are respectively -1.68% and -1.66%, while both have the same regression coefficient: 0.996.

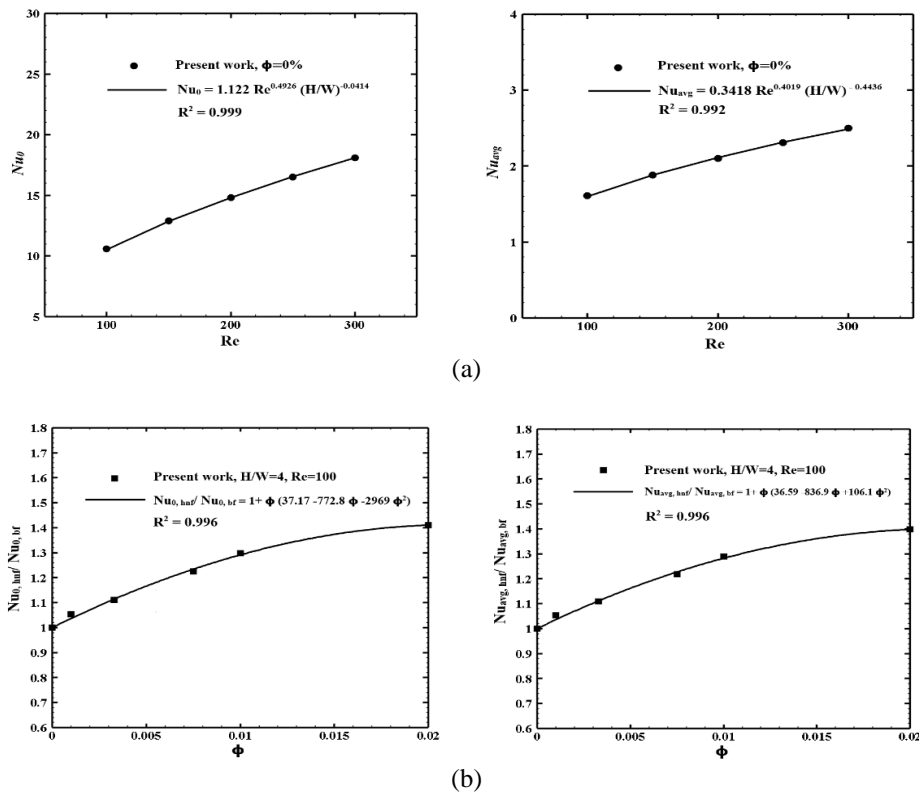


Figure 16. Suggested correlations for the stagnation point and the average Nu : a) as a function of Re and H/W for the base fluid; b) as a function of ϕ for hybrid nanofluid

CONCLUSIONS

This study attempted to design and execute a numerical simulation to study and examine the dynamic and thermal behavior of Al_2O_3 /water nanofluid and Al_2O_3 -Cu/water hybrid nanofluid flows in a confined impinging slot jet. The simulation was conducted under a Re range of $100 \leq Re \leq 300$, while the range of nanoparticles volume fraction was $0 \leq \phi \leq 2\%$. The study utilized the two-phase mixture model for the numerical simulation considering 2, 4, and 6 as the aspect ratios for investigating the confining effects. Based on results, it was concluded that heat transfer for each Reynolds number increases significantly with increasing the volume fraction of nanoparticles (for any value of Re , the heat transfer greatly increased in response to an increase in the volume fraction of the nanoparticles volume fraction). Also; following a comparison between hybrid nanofluid and nanofluid, the study found that the Nu in hybrid nanofluid is higher. Besides; as the solid volume concentration of nanofluid and hybrid nanofluid increased, the pumping power ratio increased in response, based on the numerical results. This ratio also increased with volume fraction in the experiment. In fact; for $100 \leq Re \leq 300$, the pumping powers required for the nanofluid are 1.16, 1.28, and 1.30 times higher than the values calculated for the base fluid for $\phi = 0.33, 1, \text{ and } 2\%$, respectively, while these values for the hybrid nanofluid are respectively 2.09, 6.22, and 10 times higher. Moreover, this study set the following conditions for the proposed correlations for the stagnation point and average Nusselt numbers and hybrid nanofluid: $100 \leq Re \leq 300$, $2 \leq H/W \leq 6$, and $0\% \leq \phi \leq 2\%$.

ACKNOWLEDGMENTS

The authors would like to acknowledge National Science and Engineering Research Council (NSERC), Ministry of Higher Education Malaysia and Universiti Malaysia Pahang for research grants and funding.

REFERENCES

- [1] G. Di Lorenzo, O. Manca, S. Nardini, and D. Ricci, "Numerical study of laminar confined impinging slot jets with nanofluids," *Advances in Mechanical Engineering*, vol. 4, p. 248795, 2012.
- [2] V. A. Chiriac and A. Ortega, "A numerical study of the unsteady flow and heat transfer in a transitional confined slot jet impinging on an isothermal surface," *International Journal of Heat and Mass Transfer*, vol. 45, pp. 1237-1248, 2002.
- [3] X. Li, J. L. Gaddis, and T. Wang, "Multiple flow patterns and heat transfer in confined jet impingement," *International Journal of Heat and Fluid Flow*, vol. 26, pp. 746-754, 2005.
- [4] A. Sivasamy, V. Selladurai, and P. Rajesh Kanna, "Numerical simulation of two-dimensional laminar slot-jet impingement flows confined by a parallel wall," *International Journal for Numerical Methods in Fluids*, vol. 55, pp. 965-983, 2007.

- [5] H. Lee, b. Yoon, and M. Ha, "A numerical investigation on the fluid flow and heat transfer in the confined impinging slot jet in the low Reynolds number region for different channel heights," *International Journal of Heat and Mass Transfer*, vol. 51, pp. 4055-4068, 2008.
- [6] D. Benmouhoub and A. Mataoui, "Heat transfer control of an impinging inclined slot jets on a moving wall," *Heat Transfer—Asian Research*, vol. 44, pp. 568-584, 2015.
- [7] O. Manca, D. Ricci, S. Nardini, and G. Di Lorenzo, "Thermal and fluid dynamic behaviors of confined laminar impinging slot jets with nanofluids," *International Communications in Heat and Mass Transfer*, vol. 70, pp. 15-26, 2016.
- [8] H. Lamraoui, K. Mansouri, and R. Saci, "Numerical investigation on fluid dynamic and thermal behavior of a non-Newtonian Al_2O_3 -water nanofluid flow in a confined impinging slot jet," *Journal of Non-Newtonian Fluid Mechanics*, vol. 265, pp. 11-27, 2019.
- [9] B. Yousefi-Lafouraki, A. Ramiar, and A. A. Ranjbar, "Modeling of two-phase particulate flows in a confined jet with a focus on two-way coupling," *Particuology*, vol. 39, pp. 78-87, 2018.
- [10] O. Abdelrehim, A. Khater, A. Mohamad, and A. Radwan, "Two-phase simulation of nanofluid in a confined single impinging jet," *Case Studies in Thermal Engineering*, vol. 14, p. 100423, 2019.
- [11] M. Abhijith and K. Venkatasubbaiah, "Numerical investigation of jet impingement flows with different nanofluids in a mini channel using Eulerian-Eulerian two-phase method," *Thermal Science and Engineering Progress*, p. 100585, 2020.
- [12] D. H. Lee, H. J. Park, and P. Ligrani, "Milliscale confined impinging slot jets: Laminar heat transfer characteristics for an isothermal flat plate," *International Journal of Heat and Mass Transfer*, vol. 55, pp. 2249-2260, 2012.
- [13] D. H. Lee, S. J. Kim, Y. H. Kim, and H. J. Park, "Heat transfer with fully developed slot jets impinging on confined concave and convex surfaces," *International Journal of Heat and Mass Transfer*, vol. 88, pp. 218-223, 2015.
- [14] J. Lv, S. Chang, C. Hu, M. Bai, P. Wang, and K. Zeng, "Experimental investigation of free single jet impingement using Al_2O_3 -water nanofluid," *International Communications in Heat and Mass Transfer*, vol. 88, pp. 126-135, 2017.
- [15] S. D. Barewar, S. Tawri, and S. S. Chougule, "Heat transfer characteristics of free nanofluid impinging jet on flat surface with different jet to plate distance: An experimental investigation," *Chemical Engineering and Processing-Process Intensification*, vol. 136, pp. 1-10, 2019.
- [16] B. Takabi and S. Salehi, "Augmentation of the heat transfer performance of a sinusoidal corrugated enclosure by employing hybrid nanofluid," *Advances in Mechanical Engineering*, vol. 6, p. 147059, 2014.
- [17] S. Suresh, K. Venkataraj, P. Selvakumar, and M. Chandrasekar, "Synthesis of Al_2O_3 -Cu/water hybrid nanofluids using two step method and its thermo physical properties," *Colloids and Surfaces A: Physicochemical and Engineering Aspects*, vol. 388, pp. 41-48, 2011.
- [18] W. Safiei, M. Rahman, A. Yusoff, and M. Radin, "Preparation, stability and wettability of nanofluid: A review," *Journal of Mechanical Engineering and Sciences*, vol. 14, pp. 7244-7257, 2020.
- [19] W. Azmi, S. Zainon, K. Hamid, and R. Mamat, "A review on thermo-physical properties and heat transfer applications of single and hybrid metal oxide nanofluids," *Journal of Mechanical Engineering and Sciences*, vol. 13, pp. 5182-5211, 2019.
- [20] A. Khan and M. Ali, "Thermo-hydraulic behavior of alumina/silica hybrid nanofluids through a straight minichannel heat sink," *Case Studies in Thermal Engineering*, vol. 31, p. 101838, 2022.
- [21] P. T. Kapen, C. G. N. Ketchate, D. Fokwa, and G. Tchien, "Linear stability analysis of (Cu- Al_2O_3)/water hybrid nanofluid flow in porous media in presence of hydromagnetic, small suction and injection effects," *Alexandria Engineering Journal*, vol. 60, pp. 1525-1536, 2021.
- [22] V. M. Krishna, M. S. Kumar, R. Muthalagu, P. S. Kumar, and R. Mounika, "Numerical study of fluid flow and heat transfer for flow of Cu- Al_2O_3 -water hybrid nanofluid in a microchannel heat sink," *Materials Today: Proceedings*, vol. 49, pp. 1298-1302, 2022.
- [23] M. Manninen, V. Taivassalo, and S. Kallio, "On the mixture model for multiphase flow," ed: Technical Research Centre of Finland Finland, 1996.
- [24] L. Schiller and Z. Naumann, "VDI Zeitung 1935," *Drag Coeff. Correl*, vol. 77, pp. 318-320, 1935.
- [25] K. Khanafer, K. Vafai, and M. Lightstone, "Buoyancy-driven heat transfer enhancement in a two-dimensional enclosure utilizing nanofluids," *International Journal of Heat and Mass Transfer*, vol. 46, pp. 3639-3653, 2003.
- [26] C. H. Chon, K. D. Kihm, S. P. Lee, and S. U. Choi, "Empirical correlation finding the role of temperature and particle size for nanofluid (Al_2O_3) thermal conductivity enhancement," *Applied Physics Letters*, vol. 87, p. 153107, 2005.
- [27] N. Masoumi, N. Sohrabi, and A. Behzadmehr, "A new model for calculating the effective viscosity of nanofluids," *Journal of Physics D: Applied Physics*, vol. 42, p. 055501, 2009.